Interplay between anisotropic strain, ferroelectric, and antiferromagnetic textures in highly compressed BiFeO_3 epitaxial thin films

Amr Abdelsamie, Arthur Chaudron, Karim Bouzehouane, Pauline Dufour, Aurore Finco, Cécile Carrétéro, Vincent Jacques, Stéphane Fusil, Vincent Garcia

Interplay between anisotropic strain, ferroelectric and antiferromagnetic textures in highly-compressed $BiFeO_3$ epitaxial thin films

Amr Abdelsamie[1,2], Arthur Chaudron[1], Karim Bouzehouane[1], Pauline Dufour[1], Aurore Finco[2], Cécile Carrétéro[1], Vincent Jacques[2], Stéphane Fusil[1], Vincent Garcia[1*]

AFFILIATIONS

[1]*Laboratoire Albert Fert, CNRS, Thales, Université Paris-Saclay, 91767 Palaiseau, France*

[2]*Laboratoire Charles Coulomb, Université de Montpellier and CNRS, 34095 Montpellier, France*

[*]Corresponding author: vincent.garcia@cnrs-thales.fr

ABSTRACT

$BiFeO_3$ thin films were epitaxially grown on (110)- and (001)-oriented $NdGaO_3$ single crystal orthorhombic substrates by pulsed laser deposition. The films grown on $NdGaO_3$(110) are fully strained and show two ferroelectric variants that arrange in a stripe domain pattern with 71° domain walls, as revealed by piezoresponse force microscopy. We explored their antiferromagnetic textures using scanning NV magnetometry. Surprisingly given the large compressive strain state, the films still show a spin cycloid, resulting in a periodic zig-zag magnetic pattern due to the two ferroelastic variants. The films grown on $NdGaO_3$(001) are also fully strained, but the (001) orthorhombic substrate imposes a strongly anisotropic in-plane strain. As a consequence, the ferroelectric polarization exhibits a uniaxial in-plane component, parallel to the b-axis of the substrate. The ferroelectric domain pattern consists of 109° charged domain walls between the two selected ferroelastic variants. This anisotropic strain impacts the magnetic state of $BiFeO_3$ and leads to a simpler spin texture defined by a single propagation vector for the spin cycloid. In both cases, electric-field control of ferroelectric domains tends to favor a transition to a canted antiferromagnetic order. These results reveal that the cycloidal structure of $BiFeO_3$ can undergo large compressive strain and open further electrical means to tune the magnetic state of this room-temperature multiferroic compound.

Bismuth ferrite ($BiFeO_3$) is the most famous multiferroic material, exhibiting both a large ferroelectric polarization of 100 $\mu C/cm^2$ (Ref. [1,2]) and a non-collinear antiferromagnetic order at room-temperature[3,4]. This material is the core element foreseen for the future logic-in-memory device designed by INTEL[5,6], due to its potential for low-power magnetoelectric control of magnetism via ferroelectricity.

The main magnetic interaction in $BiFeO_3$ is super-exchange, leading to a G-type antiferromagnetic order with a Néel temperature of 640 K in the bulk[7]. In addition, the magnetoelectric interaction favors a canting between adjacent Fe spins, giving rise to an incommensurate spin cycloid rotating in a plane defined by its propagation vector k, along one of the three <-110> high symmetry axes of the (111) plane, and the polarization along [111], with a period of 62-64 nm in the bulk[3,4]. A second Dzyaloshinskii-Moriya interaction, related to the antiferrodistortive tilts of the oxygen octahedra[8], results in the wiggling of the cycloid in the form of a spin-density wave with its period locked to that of the spin cycloid[9].

Epitaxial strain leads to a modification of the magneto-crystalline anisotropy of $BiFeO_3$ and therefore profoundly affects its magnetism. Despite extensive studies since its rediscovery 20 years ago[1], $BiFeO_3$ is a never-ending fascinating playground. Indeed, first expected to be ferromagnetic when grown as epitaxial thin films[1], $BiFeO_3$ was later assumed to be in a canted antiferromagnetic state[10,11]. Nevertheless, neutron scattering, macroscopic Mossbauer and Raman spectroscopy experiments revealed that (001) $BiFeO_3$ thin films actually harbor the bulk-like antiferromagnetic spin cycloid when grown under low compressive strain, display an exotic cycloid at low tensile strain, and only turn into a canted antiferromagnetic state for large tensile and compressive strain[12–14].

Recently, real-space imaging based on a single nitrogen-vacancy (NV) defect incorporated in a diamond tip has enabled imaging the antiferromagnetic spin textures of $BiFeO_3$ at the scale of ferroelectric domains and domain walls[15–19]. It turned out that low compressive strain (i.e., when grown on $DyScO_3$) favors the bulk-like (type I) spin cycloid with a one-to-one imprint of the ferroelectric domains onto the cycloidal domains and a deterministic control of the propagation vector direction with the electric field[15]. At low tensile strain (on $GdScO_3$) but also at large compressive strain (on $SrTiO_3$), the propagation vectors of the cycloid change to <-211> directions, defining it as an exotic (type II) cycloid[17]. For larger tensile strain (on $SmScO_3$), either a type II cycloid [18] or a collinear antiferromagnetic state [17] have been observed, suggesting that $BiFeO_3$ is reaching its strain-induced boundary between cycloidal and collinear antiferromagnetic states. Here we investigate the spin textures of $BiFeO_3$ thin films subjected to a larger compressive strain, i.e., on $NdGaO_3$ substrates, in order to look for the other side of the magnetic vs strain phase diagram.

$BiFeO_3$ thin films were grown by pulsed laser deposition with a KrF excimer laser on (001) and (110) orthorhombic $NdGaO_3$ single crystals. Prior to the deposition, the $NdGaO_3$ substrates were annealed in O_2 dynamic atmosphere at 1000 °C for 3 hours. With in-situ RHEED monitoring, ultrathin $La_{0.7}Sr_{0.3}MnO_3$ thin films were grown as buffer electrodes at 750 °C in oxygen pressure of 0.4 mbar. To grow the $BiFeO_3$ films, the substrate was heated to 660 °C under 0.36 mbar of oxygen environment. The laser fluence was maintained at 1 mJ/cm^2 and 1.5 mJ/cm^2 for $BiFeO_3$ and $La_{0.7}Sr_{0.3}MnO_3$, respectively, while a repetition rate of 5 Hz is adopted for both materials.

The structural properties of the films were investigated using a Rigaku Smartlab diffractometer. 2θ-ω diffraction patterns indicate that both $BiFeO_3$ thin films are single phase and Laue fringes attest for their high crystalline quality for a thickness of 45 nm (Figs. 1(b) and 3(b)). The (001) peak position at 21.2° for both films correspond to an out-of-plane lattice spacing of 0.418 nm. In order to gain deeper insights into the epitaxial strain of the films and to determine the number of ferroelastic variants in each film configuration, asymmetric reciprocal space maps (RSMs) were performed (Figs. 1(c) and 3(c)). The $NdGaO_3$ substrate is displayed in its orthorhombic structure while $BiFeO_3$ is analyzed in its monoclinic structure with the in-plane component of polarization aligned parallel to its a axis.

In the first case where $BiFeO_3$ is grown on $NdGaO_3$(110), RSMs around $NdGaO_3$(24-2), (332) and (240) indicate that $BiFeO_3$ is fully strained and possesses only two ferroelastic variants (Fig. 1(c)). As sketched in Fig. 1(a), the two ferroelastic variants are rotated by 90° in the plane and symmetric with respect to the in-plane direction of $NdGaO_3$(110) perpendicular to its c axis. This is similar to what has been already observed for $BiFeO_3$ thin films epitaxially grown on (110) orthorhombic scandates such as $DyScO_3$, $GdScO_3$ or $SmScO_3$, where the substrate symmetry lifts the degeneracy between the four ferroelastic variants and stabilizes striped-domain structures with 71° domain walls[17]. By analyzing the $BiFeO_3$ peak positions in the RSMs, we estimate the in-plane epitaxial strain to be -2.67$\pm$0.02%, corresponding to a highly-compressed $BiFeO_3$ thin film.

The ferroelectric domain structure of the films was investigated using piezoresponse force microscopy (PFM) in a Nanoscope V multimode (Bruker). As anticipated from X-ray diffraction, the films on $NdGaO_3$(110) display a stripe domain pattern with 71° domain walls (Figure 2(b)).

Vertical PFM indicates a single out-of-plane component of polarization pointing upwards, as systematically observed when $BiFeO_3$ is grown on a $La_{0.7}Sr_{0.3}MnO_3$ buffer electrode[20]. In this polar configuration, the in-plane component of polarization rotates by 90° from one domain to another (sketch in Fig. 2(a)). We studied the antiferromagnetic order of the films using two commercial scanning NV magnometers (ProteusQ from Qnami and Quantum Scanning Microscope from Qzabre). Given the large compressive strain, one would expect the spin cycloid to be unfavorable, as suggested by formerly-reported macroscopic measurements[13]. As displayed in Fig. 2(c), the periodic modulation of the magnetic stray field attests for the presence of a spin cycloid. The two ferroelectric variants result in two different propagation vectors which form the observed zig-zag pattern. The analysis of the propagation directions indicates a type II cycloid with k' vectors along [1-21] and [-211], reminiscent of what was actually observed at lower compressive strain on $SrTiO_3(001)$[17]. However, given the angle distribution of 87-107° between the propagation vectors, we cannot completely discard the presence of the type I cycloid with k_1 in-plane vectors[17]. For such a strain, the cycloidal period strongly diverges to about 110 ± 20 nm.

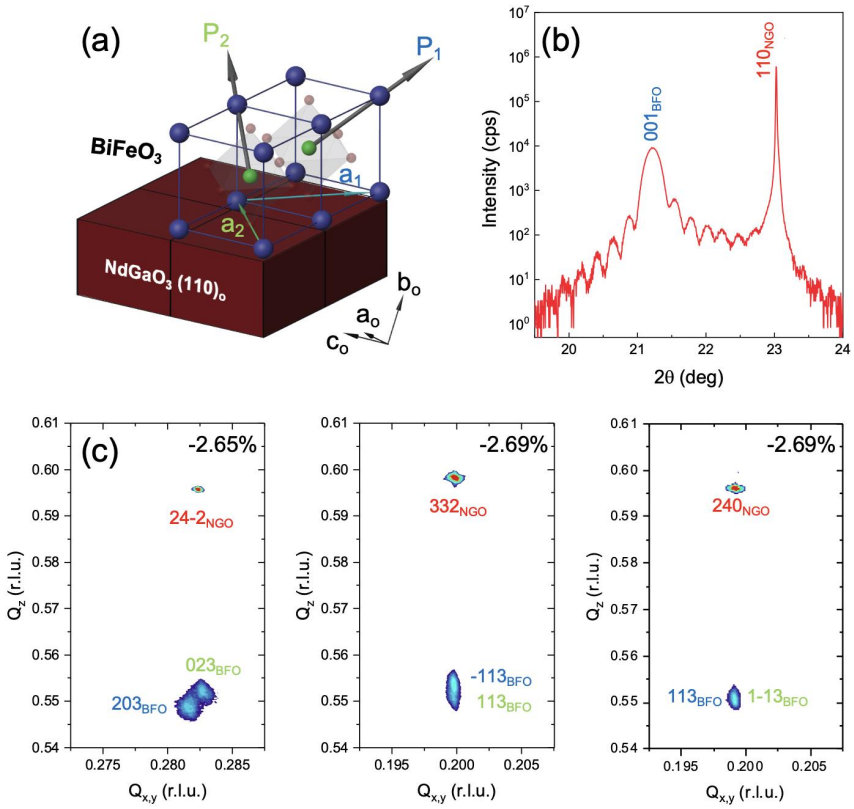

FIG. 1. Structural characterization of the $BiFeO_3$ thin films grown on (110)-oriented $NdGaO_3$ orthorhombic single crystals. (a) Sketch of the epitaxial relationships between $BiFeO_3$ and $NdGaO_3$(110). a_o, b_o and c_o are the orthorhombic axes of the substrate. Two ferroelastic monoclinic domains are displayed with a_1 and a_2 axes for each ferroelectric polarization P_1 and P_2, respectively. (b) 2θ-ω X-ray diffraction pattern around $NdGaO_3$(110). (c) Asymmetric reciprocal space maps collected around several substrate peaks. The two ferroelastic variants are indicated in blue and green and the substrate in red. NGO and BFO stand for $NdGaO_3$ and $BiFeO_3$, respectively. The indices correspond to the orthorhombic and monoclinic notations for $NdGaO_3$ and $BiFeO_3$.

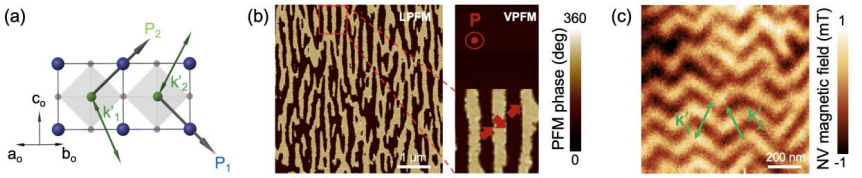

FIG. 2. Ferroelectric and antiferromagnetic textures of the $BiFeO_3$ thin films grown on (110)-oriented $NdGaO_3$. (a) 2D sketch of the projected in-plane ferroelectric and antiferromagnetic configurations. Each ferroelectric variant, P_1 and P_2, correspond to a cycloidal propagation vector, k_2' and k_1', respectively. (b) Lateral (L) and vertical (V) PFM phase images showing two ferroelectric variants alternated in a striped domain structure with 71° domain walls. VPFM indicates a homogeneous signal corresponding to a polarization component pointing upward. The in-plane polarization variants are indicated by red arrows in the zoomed image. (c) Scanning NV magnetometry image showing a zig-zag pattern with two alternated cycloidal domains. These cycloid propagation directions are sketched in (a).

In the second case where $BiFeO_3$ is grown on $NdGaO_3$(001), RSMs around $NdGaO_3$(206), (026) and (116) indicate that $BiFeO_3$ is also fully strained, again harboring two ferroelastic variants (Fig. 3(c)) with the polarization contained in the (100) plane of $NdGaO_3$ (sketch in Fig. 3(a)). This is visible from the RSM around $NdGaO_3$(026), where the two peaks of $BiFeO_3$ are split in the vertical direction, corresponding to (203) and (-203) orientations (Fig. 3(c), middle). Around $NdGaO_3$(206), the two variants merge in a single peak corresponding to (023) and (0-23) (Fig. 3(c), left). This implies a mirror symmetry with respect to $NdGaO_3$(010) for these two

ferroelastic domains rotated by 109°. Moreover, though the average epitaxial strain (-2.57%) is similar to the case of $NdGaO_3$(110), it is strongly anisotropic for the monoclinic cell with strain magnitudes of -3.2% and -1.9% along the in-plane a and b axes of $NdGaO_3$(001), respectively.

These two ferroelastic variants are also visible from piezoresponse force microscopy (Fig. 4(b)). Similarly to the previous case, vertical PFM indicates a single out-of-plane variant pointing upwards whereas lateral PFM shows two variants. Vector PFM confirms that the in-plane polarization is parallel to the b-axis of the substrate. The ferroelectric stripes are not orthogonal nor parallel to this axis, which results in partially charged head-to-head and tail-to-tail domain walls (inset of Fig. 4(b)). A peculiar contrast can be observed at every second domain wall, with a very fine set of apparently charged domain walls rather than a single wall, which may be related to some kind of energetic accommodation of the polar discontinuity, as recently reported (arXiv:2309.02068). This domain wall sequence is also reminiscent of what was observed in a similar polar landscape with alternating head-to-head and tail-to-tail domain walls[21]. Therefore, we see that changing the $NdGaO_3$ substrate orientation from (110) to (001), i.e. tuning the in-plane anisotropy, has a paramount influence on the ferroelectric domain structure of the $BiFeO_3$ thin films.

In strong contrast to the previous case, the magnetic structure of this film shows a uniaxial periodic magnetic stray field, corresponding to a single vertical propagation vector for the cycloid (Fig. 4(c)). Considering the crystal structure of $BiFeO_3$, this corresponds to a type I cycloid (the same as bulk $BiFeO_3$) with a propagation vector in the film plane, i.e. along [-110] as sketched in Fig. 4(a). As both ferroelectric variants are rotated by 180° in the plane, they

share the same cycloid propagation vector direction so that ferroelectric domain walls are no longer detected in the antiferromagnetic ordering. In this film, and in resemblance to $BiFeO_3$ deposited on $NdGaO_3$(110), the quasi-single cycloid exhibits a period of around 110 nm.

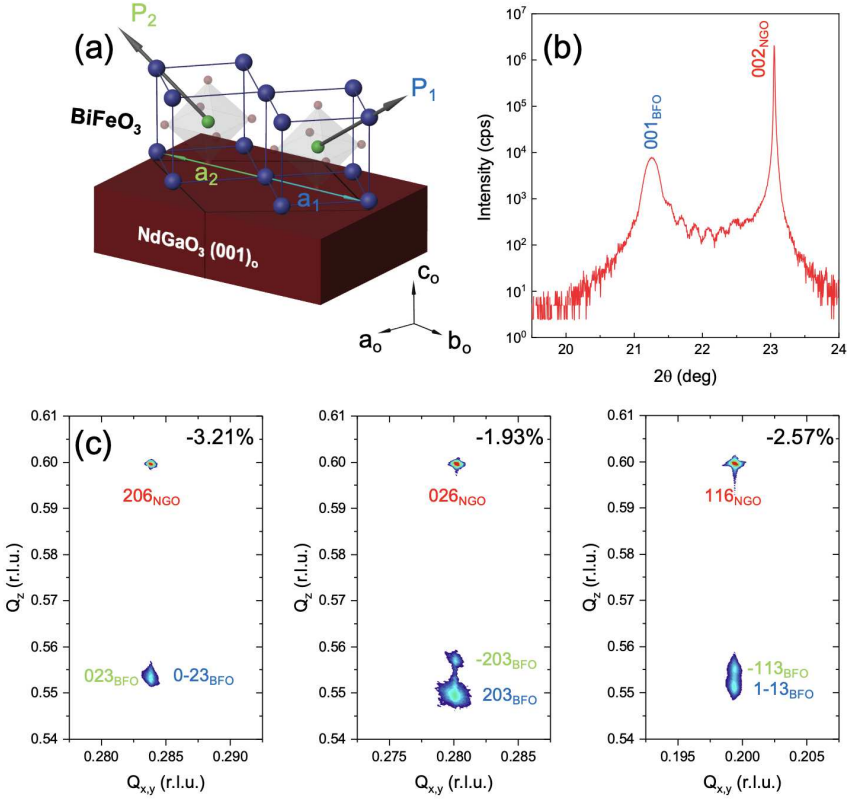

FIG. 3. Structural characterization of the $BiFeO_3$ thin films grown on (001)-oriented $NdGaO_3$ orthorhombic single crystals. (a) Sketch of the epitaxial relationships between $BiFeO_3$ and $NdGaO_3$(001). a_o, b_o and c_o are the orthorhombic axes of the substrate. Two ferroelastic monoclinic domains are displayed with a_1 and a_2 axes for each ferroelectric polarization P_1 and P_2, respectively. (b) 2θ-ω X-ray diffraction pattern. (c) Asymmetric reciprocal space maps

collected around several substrate peaks. The two ferroelastic variants are indicated in blue and green and the substrate in red. NGO and BFO stand for $NdGaO_3$ and $BiFeO_3$, respectively. The indices correspond to the orthorhombic and monoclinic notations for $NdGaO_3$ and $BiFeO_3$.

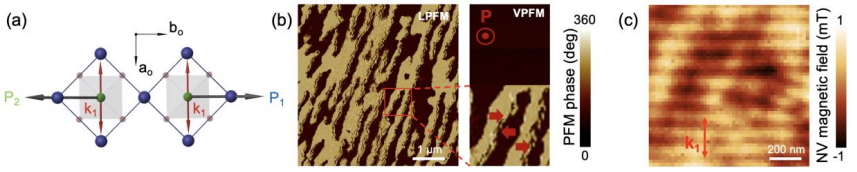

FIG. 4. Ferroelectric and antiferromagnetic textures of the $BiFeO_3$ thin films grown on (001)-oriented $NdGaO_3$. (a) 2D sketch of the in-plane ferroelectric and antiferromagnetic configurations. Each ferroelectric variant, P_1 and P_2, share the same cycloidal propagation vector, k_1. (b) Lateral (L) and vertical (V) PFM phase images showing two ferroelectric variants alternated in a striped domain structure with 71° domain walls. VPFM indicates a homogeneous signal corresponding to a polarization pointing upward. The in-plane polarization variants are indicated by red arrows in the zoomed image. (c) Scanning NV magnetometry image showing a uniform, vertically propagated cycloidal domain. Large scale patches contrasting the image stem from the intrinsic ferromagnetism of the buffer $La_{0.7}Sr_{0.3}MnO_3$ electrode.

We now turn to the electric-field manipulation of the ferroelectric domains, using the scanning PFM tip, and its influence on the antiferromagnetic textures. For the case of $BiFeO_3$ films grown on $NdGaO_3$(110), switching from pristine upward to downward polarization with the trailing field of the PFM tip[22] does not stabilize single ferroelectric domains but rather induce ferroelectric stripes rotated by 90° (LPFM at 0 and 90° in Fig. 5(a)). Scanning NV magnetometry shows that the zig-zag pattern of the type II cycloid also rotates by 90° (bottom left side of the

dashed area) but some parts of the written domains rather show a non-periodic strong magnetic stray field (Fig. 5(b)). This suggests that the large compressive strain accommodated by $BiFeO_3$ drives this system on the brink to suppress the cycloid towards a pseudo collinear antiferromagnetic state. In the case of $BiFeO_3$ films grown on $NdGaO_3$(001), the uniaxial in-plane anisotropy facilitated the design of single ferroelectric domains with the trailing field of the PFM tip (absence of LPFM signal at 90° in Fig. 5(c)). In such case, we clearly observe that the electric-field manipulation of ferroelectric domains is more homogeneous, and accompanied by a transition from the cycloidal state to a non-periodic, pseudo-collinear antiferromagnetic state in the whole switched area (Fig. 5(d)). Hence, the large and anisotropic in-plane strain seems to be more efficient in destabilizing the spin cycloid of $BiFeO_3$.

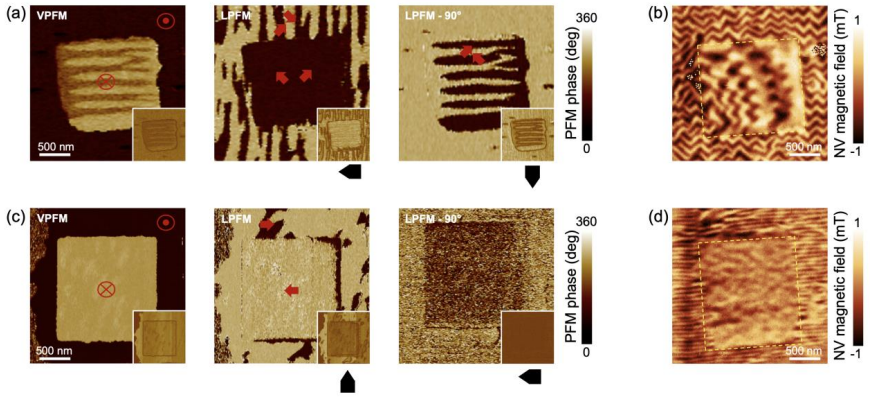

FIG. 5. Electric-field manipulation of ferroelectric domains and the resulting antiferromagnetic textures for $BiFeO_3$ thin films grown on $NdGaO_3$(110) (a-b) and $NdGaO_3$(001) (c-d). (a) & (c) Vertical and lateral PFM phase images (corresponding amplitudes in insets) of a zone with the central 2×2 μm^2 area switched to a polarization downward with a negative voltage applied to the oxide electrode. The LPFM images are displayed for 0 and 90° in-plane orientations of the samples (sketches of the corresponding PFM tip in insets). (b) & (d) Scanning NV magnetometry images of the same areas as (a) & (c), respectively, showing the surrounding as-grown magnetic states and the modified magnetic state within the dashed areas.

In summary, we investigated the spin textures in $BiFeO_3$ thin films grown under a large compressive strain on $NdGaO_3$ substrates. We found that the spin cycloid persists even if the epitaxial strain reaches more than -2.5%. In addition, homogeneous biaxial strain on $NdGaO_3$(110) promotes a striped domain structure with 71° domain walls, which gives rise to a zig-zag pattern of the exotic spin cycloid. In contrast, anisotropic strain on $NdGaO_3$(001) leads to a uniaxial arrangement of ferroelectric domains, with charged 109° domain walls, and this anisotropy triggers a single propagation vector for the spin cycloid. In both cases, the cycloidal period strongly deviates from the bulk one, suggesting a destabilization of the cycloid. Furthermore, electric-field manipulation of the ferroelectric domains results in the stabilization of collinear antiferromagnetic domains. These results bring further insights into the interplay between epitaxial strain, electric field and the antiferromagnetic order of $BiFeO_3$ thin films.

ACKNOWLEDMENTS

We are thankful for support from the French Agence Nationale de la Recherche (ANR) through the project TATOO (ANR-21-CE09-0033) and the ESR/EquipEx + program (Grant No. ANR-21-ESRE-0031), the European Union's Horizon 2020 research and innovation programme under the Grant Agreements No. 964931 (TSAR) and No. 866267 (EXAFONIS). This work is supported by a public grant overseen by the ANR as part of the "Investissements d'Avenir" program (Labex NanoSaclay, reference: ANR-10-LABX-0035). The Sesame Ile de France IMAGeSPIN project (No. EX039175) is also acknowledged.

AUTHOR DECLARATIONS

Conflict of Interest

The authors declare no conflict of interest.

DATA AVAILABILITY

The data that support the findings of this study are available from the corresponding author upon reasonable request.

REFERENCES

[1] J. Wang, J.B. Neaton, H. Zheng, V. Nagarajan, S.B. Ogale, B. Liu, D. Viehland, V. Vaithyanathan, D.G. Schlom, U.V. Waghmare, N.A. Spaldin, K.M. Rabe, M. Wuttig, and R. Ramesh, "Epitaxial $BiFeO_3$ Multiferroic Thin Film Heterostructures," Science **299**(5613), 1719–1722 (2003).
[2] D. Lebeugle, D. Colson, A. Forget, and M. Viret, "Very large spontaneous electric polarization in $BiFeO_3$ single crystals at room temperature and its evolution under cycling fields," Appl. Phys. Lett. **91**(2), 022907 (2007).
[3] I. Sosnowska, T.P. Neumaier, and E. Steichele, "Spiral magnetic ordering in bismuth ferrite," J. Phys. C: Solid State Phys. **15**(23), 4835–4846 (1982).
[4] D. Lebeugle, D. Colson, A. Forget, M. Viret, A.M. Bataille, and A. Gukasov, "Electric-Field-Induced Spin Flop in $BiFeO_3$ Single Crystals at Room Temperature," Phys. Rev. Lett. **100**(22), 227602 (2008).
[5] S. Manipatruni, D.E. Nikonov, and I.A. Young, "Beyond CMOS computing with spin and polarization," Nature Phys **14**(4), 338–343 (2018).
[6] S. Manipatruni, D.E. Nikonov, C.-C. Lin, T.A. Gosavi, H. Liu, B. Prasad, Y.-L. Huang, E. Bonturim, R. Ramesh, and I.A. Young, "Scalable energy-efficient magnetoelectric spin–orbit logic," Nature **565**(7737), 35–42 (2019).
[7] S.V. Kiselev, R.P. Ozerov, and G.S. Zhdanov, "Detection of magnetic arrangement in the $BiFeO_3$ ferroelectric by means of neutron diffraction study," Dokl. Akad. Nauk SSSR **145**(6), 1255–1258 (1962).
[8] C. Ederer, and N.A. Spaldin, "Weak ferromagnetism and magnetoelectric coupling in bismuth ferrite," Phys. Rev. B **71**(6), 060401 (2005).
[9] M. Ramazanoglu, M. Laver, W. Ratcliff, S.M. Watson, W.C. Chen, A. Jackson, K. Kothapalli, S. Lee, S.-W. Cheong, and V. Kiryukhin, "Local Weak Ferromagnetism in Single-Crystalline Ferroelectric $BiFeO_3$," Phys. Rev. Lett. **107**(20), 207206 (2011).
[10] T. Zhao, A. Scholl, F. Zavaliche, K. Lee, M. Barry, A. Doran, M.P. Cruz, Y.H. Chu, C. Ederer, N.A. Spaldin, R.R. Das, D.M. Kim, S.H. Baek, C.B. Eom, and R. Ramesh, "Electrical control of

antiferromagnetic domains in multiferroic bifeo$_3$ films at room temperature," Nature Mater **5**(10), 823–829 (2006).
[11] J.T. Heron, J.L. Bosse, Q. He, Y. Gao, M. Trassin, L. Ye, J.D. Clarkson, C. Wang, J. Liu, S. Salahuddin, D.C. Ralph, D.G. Schlom, J. Íñiguez, B.D. Huey, and R. Ramesh, "Deterministic switching of ferromagnetism at room temperature using an electric field," Nature **516**(7531), 370–373 (2014).
[12] X. Ke, P.P. Zhang, S.H. Baek, J. Zarestky, W. Tian, and C.B. Eom, "Magnetic structure of epitaxial multiferroic $BiFeO_3$ films with engineered ferroelectric domains," Phys. Rev. B **82**(13), 134448 (2010).
[13] D. Sando, A. Agbelele, D. Rahmedov, J. Liu, P. Rovillain, C. Toulouse, I.C. Infante, A.P. Pyatakov, S. Fusil, E. Jacquet, C. Carrétéro, C. Deranlot, S. Lisenkov, D. Wang, J.-M. Le Breton, M. Cazayous, A. Sacuto, J. Juraszek, A.K. Zvezdin, L. Bellaiche, B. Dkhil, A. Barthélémy, and M. Bibes, "Crafting the magnonic and spintronic response of $BiFeO_3$ films by epitaxial strain," Nature Mater **12**(7), 641–646 (2013).
[14] A. Agbelele, D. Sando, C. Toulouse, C. Paillard, R.D. Johnson, R. Rüffer, A.F. Popkov, C. Carrétéro, P. Rovillain, J.-M. Le Breton, B. Dkhil, M. Cazayous, Y. Gallais, M.-A. Méasson, A. Sacuto, P. Manuel, A.K. Zvezdin, A. Barthélémy, J. Juraszek, and M. Bibes, "Strain and Magnetic Field Induced Spin-Structure Transitions in Multiferroic $BiFeO_3$," Adv. Mater. **29**(9), 1602327 (2017).
[15] I. Gross, W. Akhtar, V. Garcia, L.J. Martínez, S. Chouaieb, K. Garcia, C. Carrétéro, A. Barthélémy, P. Appel, P. Maletinsky, J.-V. Kim, J.Y. Chauleau, N. Jaouen, M. Viret, M. Bibes, S. Fusil, and V. Jacques, "Real-space imaging of non-collinear antiferromagnetic order with a single-spin magnetometer," Nature **549**(7671), 252–256 (2017).
[16] J.-Y. Chauleau, T. Chirac, S. Fusil, V. Garcia, W. Akhtar, J. Tranchida, P. Thibaudeau, I. Gross, C. Blouzon, A. Finco, M. Bibes, B. Dkhil, D.D. Khalyavin, P. Manuel, V. Jacques, N. Jaouen, and M. Viret, "Electric and antiferromagnetic chiral textures at multiferroic domain walls," Nature Materials **19**(4), 386–390 (2020).
[17] A. Haykal, J. Fischer, W. Akhtar, J.-Y. Chauleau, D. Sando, A. Finco, F. Godel, Y.A. Birkhölzer, C. Carrétéro, N. Jaouen, M. Bibes, M. Viret, S. Fusil, V. Jacques, and V. Garcia, "Antiferromagnetic textures in $BiFeO_3$ controlled by strain and electric field," Nature Communications **11**(1), 1704 (2020).
[18] H. Zhong, A. Finco, J. Fischer, A. Haykal, K. Bouzehouane, C. Carrétéro, F. Godel, P. Maletinsky, M. Munsch, S. Fusil, V. Jacques, and V. Garcia, "Quantitative Imaging of Exotic Antiferromagnetic Spin Cycloids in $BiFeO_3$ Thin Films," Phys. Rev. Applied **17**(4), 044051 (2022).
[19] P. Dufour, A. Abdelsamie, J. Fischer, A. Finco, A. Haykal, M.F. Sarott, S. Varotto, C. Carrétéro, S. Collin, F. Godel, N. Jaouen, M. Viret, M. Trassin, K. Bouzehouane, V. Jacques, J.-Y. Chauleau, S. Fusil, and V. Garcia, "Onset of Multiferroicity in Prototypical Single-Spin Cycloid $BiFeO_3$ Thin Films," Nano Lett. **23**(19), 9073–9079 (2023).
[20] A. Abdelsamie, L. You, L. Wang, S. Li, M. Gu, and J. Wang, "Crossover between Bulk and Interface Photovoltaic Mechanisms in a Ferroelectric Vertical Heterostructure," Phys. Rev. Appl. **17**(2), 024047 (2022).
[21] E. Gradauskaite, Q.N. Meier, N. Gray, M.F. Sarott, T. Scharsach, M. Campanini, T. Moran, A. Vogel, K. Del Cid-Ledezma, B.D. Huey, M.D. Rossell, M. Fiebig, and M. Trassin, "Defeating depolarizing fields with artificial flux closure in ultrathin ferroelectrics," Nat. Mater. **22**(12), 1492–1498 (2023).
[22] N. Balke, S. Choudhury, S. Jesse, M. Huijben, Y.H. Chu, A.P. Baddorf, L.Q. Chen, R. Ramesh,

and S.V. Kalinin, "Deterministic control of ferroelastic switching in multiferroic materials," Nature Nanotech **4**(12), 868–875 (2009).